

# Deep Density-aware Count Regressor

CHEN ZHUOJUN georgechenzj@outlook.com

Confidential submitted paper

For presentation by the author CHEN ZHUOJUN only. Do not distribute

## Abstract

We seek to improve crowd counting as we perceive the limits of currently prevalent counting by density map estimation approach on both prediction accuracy and time efficiency. We propose a novel deep CNN which focuses on predicting a more accurate global count while optionally producing multi-scale density maps in a much more efficient way. We introduce multilayer gradient fusion for training a density-aware count regressor. More specifically, on training stage, a backbone network receives gradients from multiple branches to learn the density information, whereas those branches are to be detached to accelerate inference. By taking advantages of such method, our model outperforms the state-of-the-art methods with 27.5%, 2.7% and 14.3% lower MAE on UCF-QNRF, Shanghai Tech Part A and Part B datasets respectively. Our code and models will be publicly available at: [https://github.com/\[anonymised\]](https://github.com/[anonymised]).

## 1. Introduction

Crowd counting is a task to count people in image. It is mainly used in real-life for automated public monitoring such as surveillance and traffic control. In recent years, crowd counting has drawn much more attention from computer vision researchers and has been in significant progress. However, the task is riddled with many challenges due to the presence of various complexities such as non-uniform density, intra- and inter-scene variations in scale and perspective, and cluttering [8, 9]. Figure 1 illustrates some of those challenging scenarios.

Early methods [1,10,12,22,34] attempt to solve crowd counting problem by detecting each individual pedestrian in the crowd. These methods often perform poorly in the face of the above-mentioned conditions. The recent development of crowd counting comes from DNN-based methods which have achieved commendable performance. These methods [4,5,6,7] concentrate on generating the demanding density maps before integrating them to the count. They are therefore categorised into density map-based methods. However, density maps have yet, in effect, to show too much importance in practice except for



Figure 1. Representative images for challenges of non-uniform density, intra- and inter-scene variations in scale and perspective, and cluttering. In the figure, GT. means ground truth and P. means prediction made by out method.

opportunely providing for demonstration, but are expensive to compute, and their quality is difficult to guarantee. Meanwhile, methods that regress the global count directly have remained untouched in research frontiers for a while.

There is evidence in [29] suggesting that direct count regression may have comparable performance to density map-based methods. Raising state-of-the-art performances in many works, density maps have shown undeniable contribution to the improvement of count prediction. One advantage of density map-based methods may be that information with respect to location, scale alike is fed to the network through density supervision. Consequently, multi-scale or multi-column architectures [4,5,11,15] are usually adopted to fuse features from different scales to capture these kinds of information.

Still, there exists two main drawbacks: first, computational cost drastically increases along with the growth of number of columns; second, useful information learned by the low-level detectors might be lost through forward propagation. Likewise, the supervision information contained in gradients would be attenuated through backward propagation, making low-level detectors difficult to learn.

To address these problems, we propose a novel Gradient Fusion based model called DeepCount for crowd counting (network architecture shown in Figure 2), making efforts to both avert expenditure of multi-column architecture and improve precision. As in Figure 2, our proposed model contains a backbone network with convolution layers deeply regressing a global count. Some auxiliary modules branch out to produce density maps with a corresponding spatial dimension and to feed gradients back to the backbone. There are five branches having different depths and independent parameters so as to learn features in different aspects. For reducing information loss, each branch will directly access different levels of the backbone to inculcate knowledge to it deeply and make it more perceptive on the density distribution of the image, namely to be density-aware.

In inference phase, the backbone network can be used unaccompanied by branches as a regressor to efficiently predict the global count, or, if needed, with an auxiliary branch to also visualise a density map. Expensive computation is taken out, but with functionality promised.

Compared to other multi-column methods, our model fuses gradients other than features and avoids relying on the hard-to-produce density maps to make prediction, but instead to leverage density maps on training and dismiss them in inference. By so doing, our model is able to incorporate advantages of accuracy, flexibility, and efficiency.

Extensive experimental results on four benchmark datasets demonstrate significant improvements of our method against the state-of-the-art methods on Shanghai Tech Part A, Part B and UCF-QNRF datasets and excellent performance on Mall dataset.

The rest of the paper is structured as follow: we review literatures for crowd counting in section 2; section 3 provides the detailed interpretation of our method; section 4 reports experiment results; in section 5, we further discuss our findings and insights; the paper is to be concluded in section 6.

## 2. Related works

### 2.1. Detection-based methods

Early crowd counting methods tend to rely on detection by sliding window approach. Low-level hand-crafted features such as Histograms of Oriented Gradients, silhouette-oriented features are exploited for traditional classifiers such as Support Vector Machine and Random Forest [1, 10, 12, 22, 34]. Following are CNN-based methods (e.g. Faster R-CNN [28]) which have shown credible detection precision [23]. Nonetheless, in such times when the subject of crowd counting was more on the stage of pedestrian detection, performances of these

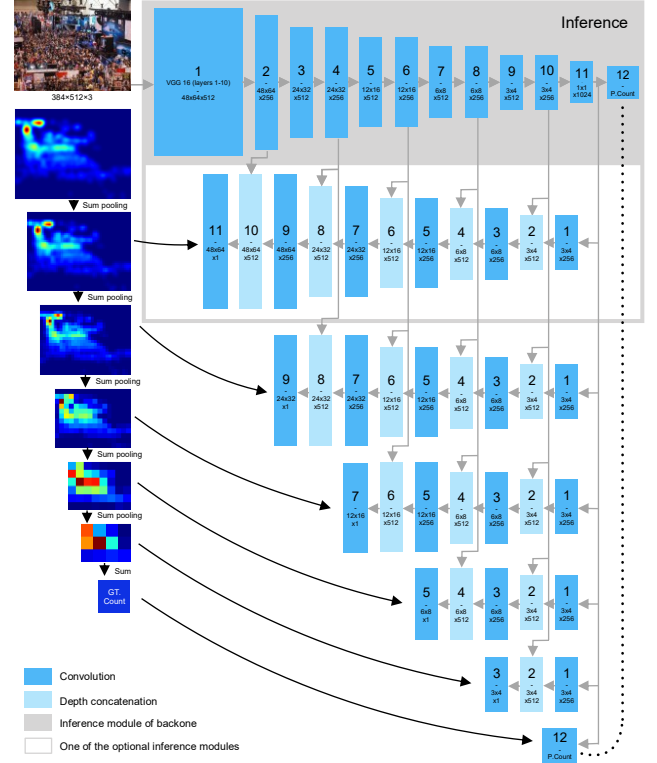


Figure 2. The architecture of the proposed DeepCount Model. Module in the grey box is the backbone regressor, below which are 5 branches predicting density maps. Large-size numbers on the blocks are referred to in detailed configuration in Table 1, while smaller ones indicate the feature map dimensions.

methods on highly dense crowd scenes were similarly limited.

### 2.2. Count regression-based methods

Count regression-based methods are proposed to overcome limits encountered by detection-based methods. The idea of these methods is to regress a global count from the input image. There are methods using ridge regression [13, 14], log-linear regression [17] or MLP [20] on low-level hand-crafted features to estimate the count. While these methods work satisfactorily on invariant scenes of sparse density, hand-crafted features can hardly represent enough variance and intricacy in complex counting scenarios. Alternatively, with the development of deep learning, features can be black-boxed and deeply learned to target the goal. Early success of applying deep learning methods on crowd counting would be the end-to-end deep CNN regression model by Wang et al. [18]. Though, deep learning methods quickly narrowed onto density map-based methods which have prevailed over the years since, and it was not until recently in [29] that Idrees et al. report excellent experiment results on global count regression by advanced CNNs: Resnet101 [25] and Densenet201 [26]. Though, their focus is still on density map-based methods.

### 2.3. Density map-based methods

Rodriguez et al. [21] first suggest the use of density map can improve crowd counting results significantly. It is supported by Zhang et al. [7] whose model produces small density map patches as well as the patch count at its last layer. Following this density map approach, Zhang et al. [4] propose a multi-column architecture (MCNN) to also address scale variance of the counting target. Inspired by such, Cao et al. [11] introduce Scale Aggregation Network (SANet) which aggregates multi-scale features and fuses them in every layer. Likewise, Switching-CNN [5] has independent columns of regressors similar to multi-column network with different receptive fields, and ic-CNN [15] aims at predicting high-resolution density maps with two branches. Another set of methods devote themselves to trace context information as well as other abstractions all in a bit to improve the predicted density maps [6, 35, 36, 37]. On the other hand, CSRNet [16] builds dilated convolution layers upon a VGG-16 [19] backbone straightforward without too many manoeuvres, yet it reports excellent results and therefore becomes more practiced at present.

Our method embodies heterogeneity of multi-column methods and straightforwardness of CSRNet, whilst appears as an existence that is both regression-based and density map-based.

## 3. DeepCount

### 3.1. Gradient Fusion

We regard our methodology of designing the network as Gradient Fusion. Multi-column methods such as MCNN [4] and CP-CNN [6] are feature fusion methods assembling different columns features from which are fused and gradients to which are separated. Fusing feature maps of multiple columns entails lots of computation since each column cannot be without in order to make prediction. In contrast, the method of gradient fusion fuses only gradient matrices in back-propagation in training, but it should still serve the purpose of fusion, which is to extract knowledge from different components. Therefore, we design branches that produce different gradient flows from density maps of different scales and fuse them together to train a critical backbone module to make better prediction. Put figuratively, with interconnections between branches and backbone, multi-source gradients filtered by branches propagating backwards find their shortcuts to penetrate into the backbone network multilayeredly when supervision is applied. This is a process that enables the backbone to be trained to summarise useful information and gain more knowledge about the representation to improve itself.

### 3.2. Network configuration

As shown in Figure 2, our proposed model consists of a

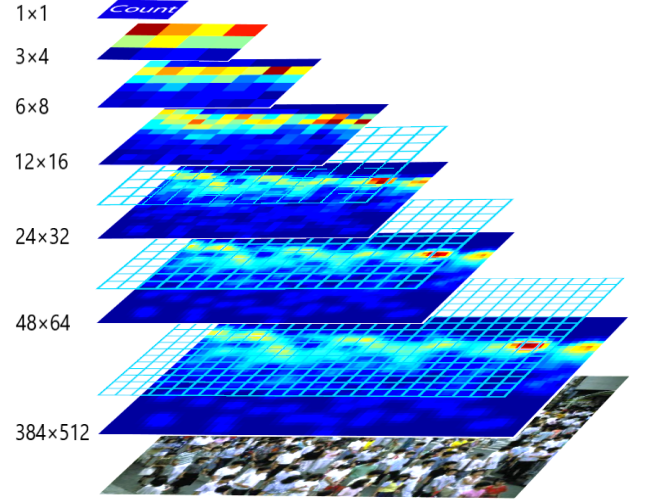


Figure 3. Illustration of sum pooling operation for density map generation.

straightforward down-sampling backbone and five branches interconnected to it. The backbone by itself has relatively low complexity. It functions as a deep CNN regressor which takes the crowd image as input and predicts the global count by regression. We design the network to have input size of  $384 \times 512$  to cater most aspect ratios in practical uses, whereas arbitrary larger input image sizes are tackled by division and combination. Correspondingly, there are density maps of sizes  $\{48 \times 64, 24 \times 32, 12 \times 16, 6 \times 8, 3 \times 4\}$  produced.

Specifically, the backbone has a frontend which extracts features from the input image. We transplant the first ten convolution layers from VGG-16 as our frontend model for faster training. The frontend produces feature maps of 8 times smaller spatial width and height relative to the input. Following are some  $3 \times 3$  convolution layers to further dwindle the size of feature maps until when its spatial dimension matches the input dimension of a  $3 \times 4$  convolution layer entering to produce a  $1 \times 1024$  vector. We use  $3 \times 3$  convolution with strides of 2 to halve the spatial dimension of the feature maps in the backend. In addition, a standard  $3 \times 3$  convolution layer is put between two down-sampling layers to further deepen the network and to smooth the reduction of features.

As for branches, they work in an up-sampling manner. Branches stemming from the last feature layer ( $1 \times 1024$ ) of the backbone use  $3 \times 4$  transposed convolution and then  $4 \times 4$  transposed convolutions to up-sample the feature maps. To the output of each transposed convolution layer, the deeper feature maps from backbone with the same dimension are appended. Together, they form the input to the next transposed convolution layer. When this concatenation has the spatial dimension that meets the target density map of the branch it is on, a  $1 \times 1$  convolution comes in to reconstruct all channels to one to produce the density map prediction. At the end of the backbone, another  $1 \times 1$



Module	Backbone	Branch 1	Branch 2	Branch 3	Branch 4	Branch 5
Input	Image 384×512×3	1×1024	1×1024	1×1024	1×1024	1×1024
1	VGG 16 Layers 1-10	Conv-tr-S1 3×4×1024×256	Conv-tr-S1 3×4×1024×256	Conv-tr-S1 3×4×1024×256	Conv-tr-S1 3×4×1024×256	Conv-tr-S1 3×4×1024×256
2	Conv-S1 3×3×512×256	Depth Concatenation	Depth Concatenation	Depth Concatenation	Depth Concatenation	Depth Concatenation
3	Conv-S2 3×3×256×512	Conv-tr-S2 4×4×512×256	Conv-tr-S2 4×4×512×256	Conv-tr-S2 4×4×512×256	Conv-tr-S2 4×4×512×256	Conv-S1 1×1×512×1
4	Conv-S1 3×3×512×256	Depth Concatenation	Depth Concatenation	Depth Concatenation	Depth Concatenation	
5	Conv-S2 3×3×256×512	Conv-tr-S2 4×4×512×256	Conv-tr-S2 4×4×512×256	Conv-tr-S2 4×4×512×256	Conv-S1 1×1×512×1	
6	Conv-S1 3×3×512×256	Depth Concatenation	Depth Concatenation	Depth Concatenation		
7	Conv-S2 3×3×256×512	Conv-tr-S2 4×4×512×256	Conv-tr-S2 4×4×512×256	Conv-S1 1×1×512×1		
8	Conv-S1 3×3×512×256	Depth Concatenation	Depth Concatenation			
9	Conv-S2 3×3×256×512	Conv-tr-S2 4×4×512×256	Conv-S1 1×1×512×1			
10	Conv-S1 3×3×512×256	Depth Concatenation				
11	Conv-S1 3×4×256×1024	Conv-S1 1×1×512×1				
12	Fc 1024×1					
Output	P. Count	P. Density Map 48×64	P. Density Map 24×32	P. Density Map 12×16	P. Density Map 6×8	P. Density Map 3×4

Table 1. Configuration of DeepCount network. In the table, Conv and Conv-tr mean convolution and transposed convolution respectively. The pattern  $H \times W \times C \times C'$  represents the dimension of convolution kernel. S denotes strides.

convolution (or fully connected layer) regresses a scalar value, the global count prediction. We call our network DeepCount in short for deep CNN count regressor. Table 1 details the network configuration.

### 3.3. Generating ground truth density maps

To produce ground truth density maps for training and validation, we first apply convolution by fixed Gaussian kernel with standard deviation  $\sigma = 5$  (on the contrary of geometry-adaptive kernel adopted in most works) to generate density map of the same resolution as the original image, before Sum Pooling is employed to produce different sizes of density maps. Sum pooling explicitly is summing all values inside a pooling window. Figure 3 illustrates this operation. As shown in Figure 3, five density maps are produced. Through sum pooling, element sum for all density maps created from one original density map stays unchanged; this sum is the ground truth count of the image.

### 3.4. Objective function

Labelling congested crowd data is indeed a painstaking task for human annotators, especially in some highly congested cases where the factual number of people is inevitably untraceable. This results in many annotations in congestions themselves being estimations, which means noise in the situation. Hence, L1-norm loss is adopted to

enhance robustness against noise as well as to convey steady updates to the network. We first define our loss function as:

$$L(\theta) = \frac{1}{2N} \sum_{n=1}^N \sum_{k=1}^K \sum_{i,j} |y'_{nk} - f(X_n, \theta_k)|_{ij} \quad (1)$$

where  $N$  is the size of the training batch,  $K$  ( $K = 6$  &  $k \in \{1, 2, \dots, 6\}$ ) enumerates outputs of all branches and the global count regressor,  $y'_{nk}$  is the ground truth density map (or the global count when  $k = 6$ ),  $X_n$  is the input image and  $\theta_k$  denotes all parameters in model  $f$  that contribute to making the corresponding  $k_{th}$  prediction.

Given this loss function as basis, we add a multiplier  $\beta$  to accentuate the importance of the global count prediction on backbone (where  $k = 6$ ). We notate it as a function of  $k$ :

$$B(k) = \begin{cases} \beta, & k = 6 \\ 1, & k \neq 6 \end{cases} \quad (2)$$

Moreover, we add another hyperparameter  $\omega$  to approximately adjust the loss to a reasonably small value ( $<10$ ). An L2 regularisation term is also added to the loss function in an attempt to reduce overfitting. Hence, the loss function finally becomes:

$$L(\theta) = \left[ \frac{1}{2N} \sum_{n=1}^N \sum_{k=1}^K \sum_{i,j} |y'_{nk} - f(X_n, \theta_k)|_{ij} \cdot B(k) \right] \cdot \omega + \frac{\lambda}{2} \|\theta\|_2^2 \quad (3)$$

### 3.5. Implementation

VGG-16 model pretrained on ImageNet is used to initialise the frontend of the backbone. Therefore, input images are normalised in the same manner as how the VGG-16 model is trained. As for initialising the remaining part of the model, we use Xavier [33] initialisation for weights and a constant value 0 for biases. With the exception of the VGG-16 frontend where ReLU is the activation function, we set parametric ReLUs (leaky ReLU):

$$a(x) = \begin{cases} x, & x > 0 \\ \alpha x, & x \leq 0 \end{cases} \quad (4)$$

following every convolution layer. We choose  $\lambda = 1 \times 10^{-5}$ ,  $\omega = 1 \times 10^{-2}$  and  $\beta = 16$  empirically for the loss function in equation (3), and  $\alpha = 0.2$  for the activation parameter in equation (4) in light of experiments reported in [31]. We use Gradient Descent optimisation with momentum 0.9 and initial learning rate  $1 \times 10^{-4}$  to train our model, except for pretrained parameters in frontend where learning rate is divided by a factor of 2 to initially  $5 \times 10^{-5}$ . Batch size  $N$  is set to 32. A hundred epochs should be enough for training.

As alluded to above, to cope with images of varied sizes, we divide the original images to  $384 \times 512$  crops to feed into our network. In inference, results from cropped images are to be merged to assemble the original image again.

## 4. Evaluation

In this section, we report evaluation results yielded by our method introduced above. We evaluate our DeepCount network on four public datasets: Shanghai Tech [4] Part A and Part B, UCF-QNRF [29] and Mall [13]. Training details for all datasets are the same as mentioned in implementation section (section 3.5). In order to make fair comparison with benchmark results, we do no more data augmentation than random cropping and mirroring during training.

### 4.1. Evaluation metrics

For evaluation, we compute mean-absolute error (MAE) and root-mean-squared error (RMSE):

$$MAE = \frac{1}{N} \sum_{i=1}^N |C_i - C_i^{GT}| \quad (5)$$

$$RMSE = \sqrt{\frac{1}{N} \sum_{i=1}^N \|C_i - C_i^{GT}\|^2} \quad (6)$$

where  $N$  is the number of testing images,  $C_i$  and  $C_i^{GT}$  meaning predicted count and ground truth count respectively.

### 4.2. Shanghai Tech

Shanghai Tech dataset [4] includes Part A and Part B. Part A is the dataset for congested crowd counting. It has 241,677 annotations in 300 training images and 182 testing images with an average number 501. On the other hand, the relatively sparse Part B is separated into training set with 400 images and testing set with 316 images taken from streets in Shanghai. Our DeepCount model achieves state-of-the-art performance on both datasets. Test results are shown in Table 2.

	Part A		Part B	
Method	MAE	RMSE	MAE	RMSE
MCNN [4]	110.2	173.2	26.4	41.3
Switching CNN [5]	90.4	135.0	21.6	33.4
DecideNet [23]	-	-	20.75	29.42
CP-CNN [6]	73.6	106.4	20.1	30.1
ic-CNN [15]	68.5	116.2	10.7	16.0
CSRNet [16]	68.2	115.0	10.6	16.0
SANet [11]	67.0	<b>104.5</b>	8.4	13.6
DeepCount (ours)	<b>65.2</b>	112.5	<b>7.2</b>	<b>11.3</b>

Table 2. Test results on Shanghai Tech Part A and Part B

### 4.3. UCF-QNRF

The UCF-QNRF [29] dataset has a greater number of annotations (1,251,642) in higher quality images of a wider variety of scenes, including sparse and dense ones. There are extremely dense scenes in this dataset, so much so that a single image may have maximumly 12,865 of annotations in UCF-QNRF. It is the most challenging one in terms of crowd density. Our method, to a great extent, outperforms current methods (see Table 3).

Method	MAE	RMSE
Idrees et al. (2013) [3]	315	508
MCNN [4]	277	426
CMTL [24]	252	514
Switching CNN [5]	228	445
Resnet101[25]	190	277
Densenet201[26]	163	226
Idrees et al. (2018) [29]	132	191
DeepCount (ours)	<b>95.7</b>	<b>167.1</b>

Table 3. Test results on UCF-QNRF.

### 4.4. Mall

Unlike the three datasets aforementioned, images from Mall dataset [13] are surveillance frames from a static viewpoint at a same venue. There are 800 frames for training and the other 1200 for testing. Crowd in this dataset is sparse. So, Mall is less challenging than others. Although

CSRNet (backend)			DeepCount Branch 1			DeepCount (backend)		
Layer	Output	Million FLOPs	Layer	Output	Million FLOPs	Layer	Output	Million FLOPs
Conv-s1 3×3×512×512	48×64×512	7248	Conv-tr-s1 3×4×1024×256	3×4×256	37	Conv-s1 3×3×512×256	48×64×256	3624
Conv-s1 3×3×512×512	48×64×512	7248	Conv-tr-s2 4×4×512×256	6×8×256	101	Conv-s2 3×3×256×512	24×32×512	906
Conv-s1 3×3×512×512	48×64×512	7248	Conv-tr-s2 4×4×512×256	12×16×256	403	Conv-s1 3×3×512×256	24×32×256	906
Conv-s1 3×3×512×256	48×64×256	3624	Conv-tr-s2 4×4×512×256	24×32×256	1611	Conv-s2 3×3×256×512	12×16×512	226
Conv-s1 3×3×256×128	48×64×128	906	Conv-tr-s2 4×4×512×256	48×64×256	6442	Conv-s1 3×3×512×256	12×16×256	226
Conv-s1 3×3×128×64	48×64×64	226	Conv-s1-p0 1×1×512×1	48×64×1	2	Conv-s2 3×3×256×512	6×8×512	57
Conv-s1 1×1×64×1	48×64×1	0.2				Conv-s1 3×3×512×256	6×8×256	57
						Conv-s2 3×3×256×512	3×4×512	14
						Conv-s1 3×3×512×256	3×4×256	14
						Conv-s1-p0 3×4×256×1024	1×1×1024	3
						Conv-s1-p0 (Fc) 1×1×1024×1	1	0.001
Total		26500			8596			6034

Table 5. Comparing between configurations and FLOPs of CSRNet and our DeepCount.

previous methods have shown very promising results on this dataset, we still evaluate our model on it to demonstrate its excellent performance on invariant scene and as well to make comparison with some detection-based methods. (see Table 4).

Method	MAE	RMSE
R-FCN [27]	6.02	5.46
Faster R-CNN [28]	5.91	6.60
COUNT Forest [30]	4.40	2.40
Weighted VLAD [32]	2.41	9.12
DecideNet [23]	<b>1.52</b>	<b>1.90</b>
DeepCount (ours)	1.55	2.00

Table 4. Test results on Mall

## 5. Discussion

### 5.1. Capacity and velocity

Arguably, the more parameters a neural network has, the greater its potential is to have high capacity to model the underlying relationship of the random variables. Although many cases suggest otherwise, we do see the positive correlation between extra parameters and increments of performance [16, 19, 25, 38]. Be that as it may, we still tend to avoid expensive computation a larger network would bear in practice. Trading off between capacity and velocity has been a dilemma for long. Hereby, we explicate how the idea of our DeepCount network is able to pursue both capacity and velocity at the same time. CSRNet [16], in whose paper Li et al. do persuasively argue about the effect of number of parameters and design efficiency, is the counterpart of our model for comparative demonstration.

CSRNet and our backbone network both have a straightforward design and use the same VGG-16 frontend, so the difference between the two lies in the backends, where CSRNet predicts the density map and our model predicts the global count. Assuming they receive the same 384×512×3 input, we detail their layer configuration with corresponding output and computation cost of each layer in Table 5. In addition, we add branch 1 which predicts the density map as same as the one predicted by CSRNet to the table. We compute computation cost in terms of floating-point operations (FLOPs) that happen throughout a forward pass in the backend. Number of FLOPs of one convolution layer is computed as:

$$FLOPs = H \cdot W \cdot C \cdot K_1 \cdot K_2 \cdot C' \quad (7)$$

where it depends multiplicatively upon output feature map size  $H \times W$ , convolution kernel size  $K_1 \times K_2$ , the number of output channels  $C$ , and the number of input channels  $C'$ .

We also measure number of parameters as well as frame-per-second (FPS) for both networks (see Table 6). Run time evaluation is performed on one NVIDIA Tesla P40 GPU. As mentioned above, the backbone of our DeepCount model can be a standalone network detached from the rest in inference, and thereby becomes a count regressor without computing the computationally expensive density maps, and noticeably, with overwhelming performance compared to other global count regression approaches.

As shown in Table 5 and Table 6, having a deeper architecture and greater preponderance of parameters (58.1 million for training and 21.4 million for inference) though, our DeepCount backbone does count inferences with much less FLOPs and therefore in higher velocity, and perhaps more importantly, with higher accuracy. These quantitative

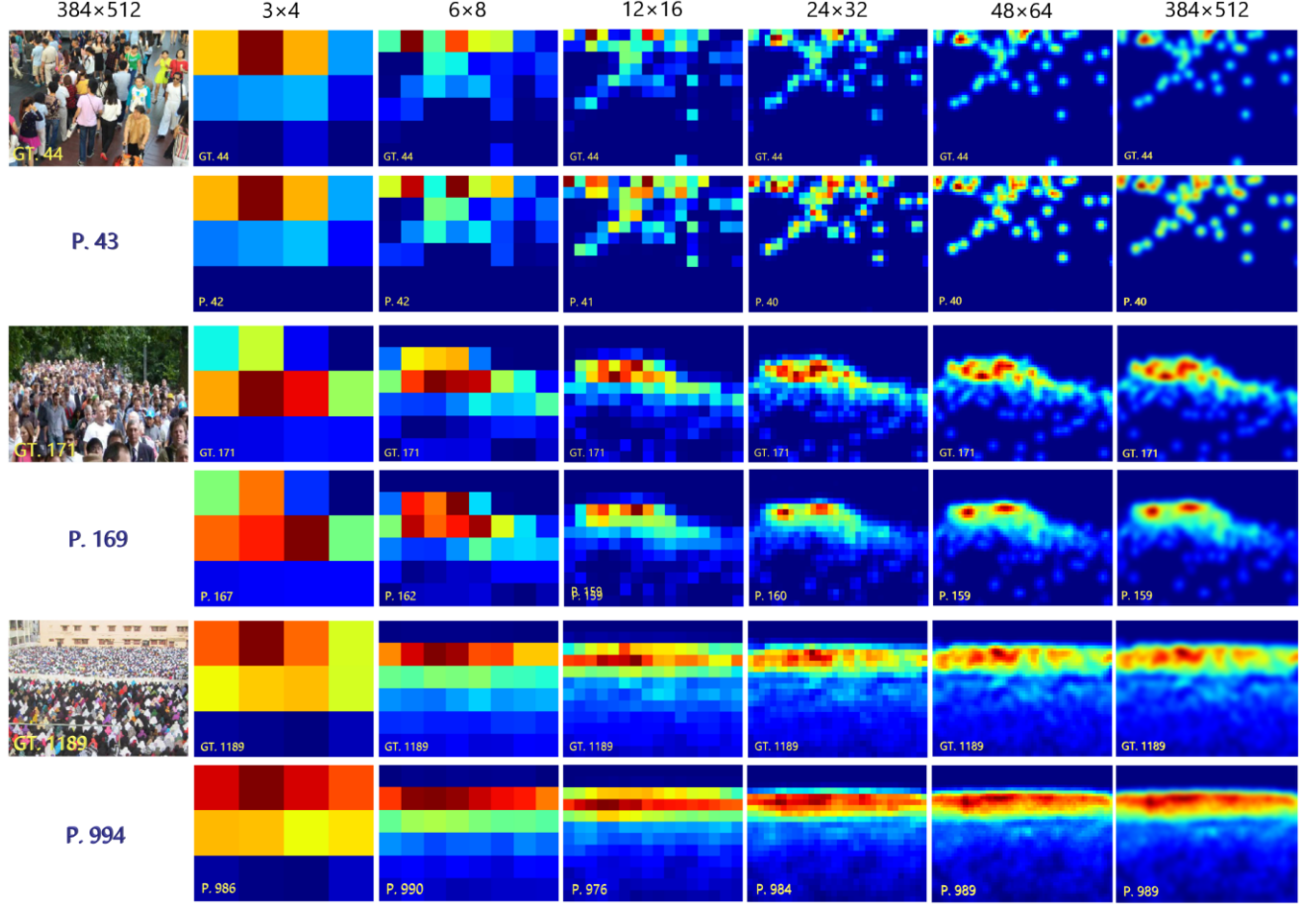


Figure 4. Examples of ground truth and output density maps of test data from Shanghai Tech Part B (top), Part A (middle), UCF-QNRF (bottom). Density maps in the row which starts with an image are the ground truths. The ones below are the predictions. The number in blue below the image is the predicted count by backbone alone. The last column shows original size ground truth density maps and predictions density maps up-sampled from outputs of branch one, up-sampling being done by bilinear interpolation and separable Gaussian filter.

results indicate our proposed DeepCount model has the ability of accommodating more variations while making faster and better prediction. This implies its potential of

Method	SHT Part B MAE	Million Parameters	FPS	Speedup
CSRNet	10.6	16.3	33	1×
DeepCount (ours)	7.2	21.4 (58.1 in total)	45	1.4×

Table 6. Comparing number of parameters and inference speed between CSRNet and the backbone of our DeepCount model.

outstanding capacity and efficiency.

## 5.2. Comparison on branches

Each branch produces a density map of a particular resolution at its end. As we have obtained the global count regressed by backbone, we can as well integrate the output density map to make count prediction like common density

map-based methods. In the following, we compare predictions made in terms of MAE between branches. Besides, we compute FLOPs for each branch to analyse their computational cost. Results are shown in Table 7.

As shown, the fact that branches that are able to produce larger density maps give inferior predictions on the count compared to those are not implies that the larger the resolution of density map, the harder it is to be optimised by the algorithm. Immediate reasons for this may be that larger density maps are sparser and usually awash with noise mostly caused by annotations of large-scale heads. Our method avoids predicting the count relying merely on density maps, but exploits useful information from them to rather train the global count regressor. This allows more accurate predictions to be achieved.

In spite of extra computation, there are situations in which density maps, which give information about the distribution, become a requirement. Our DeepCount model can make direct count inference with backbone in its full speed while optionally producing density maps of multiple



	Branch 1	Branch 2	Branch 3	Branch 4	Branch 5	Backbone
Output Size	48×64	24×32	12×16	6×8	3×4	1×1
Shanghai Tech Part A	79.2	73.4	69.7	66.7	65.8	65.2
Shanghai Tech Part B	9.7	8.9	8.0	7.4	7.2	7.2
UCF-QNRF	193.3	185.0	155.3	112.3	96.9	95.7
Mall	4.74	2.89	2.46	1.77	1.56	1.55
Million FLOPs	6034	2152	541	138	38	-

Table 7. Comparing between outputs on different branches.

resolutions. User can choose smaller density maps to reduce computational expensiveness or larger ones to give more illuminating impression about the crowd distribution. Using bilinear interpolation and separable Gaussian filter, the largest density map can be efficiently up-sampled to original resolution for high-definition display. Figure 4 shows our predicted density maps compared to their ground truths.

### 5.3. Significance of gradients

Gradients are considered crucial to the achievement of our model. Hence, we detail more experiments to further cast light on the importance of them. Since ReLU has derivatives:

$$a(x)'_{ReLU} = \begin{cases} 1, & x > 0 \\ 0, & x < 0 \end{cases} \quad (8)$$

, where gradients in half of its activation space are set to zero, the resulting sparse gradient matrices would hinder propagation of gradient flow and counterproductively cause a large part of the network underused. Instead, Parametric ReLU has derivatives:

$$a(x)'_{PReLU} = \begin{cases} 1, & x > 0 \\ \alpha, & x < 0 \end{cases} \quad (9)$$

with non-zero gradients in all quadrants which allow the network to fully learn. Table 8 shows results of training a network with all ReLU activations in comparison with our baseline network. As shown in Table 8, when gradients are sparse, the capability of the network drops.

Activation	SHT Part B MAE
ReLU	8.8
PReLU	7.2

Table 8. Comparing results between using ReLU (sparse gradients) and PReLU (full gradients).

Also, the idea of being density-aware by gradient fusion is to leverage gradients sourced from supervision of multi-

Ablation	SHT Part B MAE
No ablation	7.2
Branch 1 ablated	7.4
Branches 1-2 ablated	7.7
Branches 1-3 ablated	8.2
Branches 1-4 ablated	8.3
Branches 1-5 ablated	9.1

Table 9. Ablation on branches.

scale density maps. In ablation experiments (see Table 9 for the results), we can see that as we detach branches one by one from the largest to the smallest in training, the backbone receives less gradients in each case, and then the trend of performance degradation becomes more and more apparent.

By means of this, we are now safer to conclude that the abundance of gradients has advantageous influence on our network and parameters in branches are indeed instrumental in the training of backbone. Giant as it may be, the network of branches is not a concern in deployment for inferences. Unless training efficiency is also in a serious consideration, having a rationally greater number of parameters in this auxiliary module should be deemed innocuous as long as performance does not remain stagnant.

## 6. Conclusion

In this paper, we have discussed advantages and limitations of current crowd counting methods, in light of which we propose a novel DeepCount network to be both fast and precise on count prediction and flexible on density map generation. State-of-the-art performance on public datasets evidence the effectiveness of our method. We reckon it is also worth mentioning that our method prevailed over current state-of-the-arts on a much larger 14k-images dataset from BaiduStar2018 competition of crowd counting which could be a more convincing evidence of its accomplishments. Our code and models will be publicly available at [https://github.com/\[anonymised\]](https://github.com/[anonymised]).

## References

- [1] W. Ge and R. T. Collins, "Marked point processes for crowd counting," 2009 IEEE Conference on Computer Vision and Pattern Recognition, Miami, FL, 2009, pp. 2913-2920.
- [2] H. Idrees, K. Soomro and M. Shah, "Detecting Humans in Dense Crowds Using Locally-Consistent Scale Prior and Global Occlusion Reasoning," in IEEE Transactions on Pattern Analysis and Machine Intelligence, vol. 37, no. 10, pp. 1986-1998, 1 Oct. 2015.
- [3] H. Idrees, I. Saleemi, C. Seibert and M. Shah, "Multi-source Multi-scale Counting in Extremely Dense Crowd Images," 2013 IEEE Conference on Computer Vision and Pattern Recognition, Portland, OR, 2013, pp. 2547-2554.
- [4] Y. Zhang, D. Zhou, S. Chen, S. Gao and Y. Ma, "Single-Image Crowd Counting via Multi-Column Convolutional Neural Network," 2016 IEEE Conference on Computer



- Vision and Pattern Recognition (CVPR), Las Vegas, NV, 2016, pp. 589-597.
- [5] D. B. Sam, S. Surya and R. V. Babu, "Switching Convolutional Neural Network for Crowd Counting," 2017 IEEE Conference on Computer Vision and Pattern Recognition (CVPR), Honolulu, HI, 2017, pp. 4031-4039.
  - [6] V. A. Sindagi and V. M. Patel, "Generating High-Quality Crowd Density Maps Using Contextual Pyramid CNNs," 2017 IEEE International Conference on Computer Vision (ICCV), Venice, 2017, pp. 1879-1888.
  - [7] C. Zhang, H. Li, X. Wang and Xiaokang Yang, "Cross-scene crowd counting via deep convolutional neural networks," 2015 IEEE Conference on Computer Vision and Pattern Recognition (CVPR), Boston, MA, 2015, pp. 833-841.
  - [8] V. A. Sindagi and V. M. Patel, "A survey of recent advances in cnn-based single image crowd counting and density estimation," Pattern Recognition Letters, no. 107, pp. 3-16, 2018.
  - [9] M. S. Zitouni, H. Bhaskar, J. Dias, and M. E. Al-Mualla, "Advances and trends in visual crowd analysis: A systematic survey and evaluation of crowd modelling techniques," Neurocomputing, no. 186, pp. 139-159, 2016.
  - [10] Viola, Jones and Snow, "Detecting pedestrians using patterns of motion and appearance," Proceedings Ninth IEEE International Conference on Computer Vision, Nice, France, 2003, pp. 734-741 vol.2.
  - [11] X. Cao, Z. Wang, Y. Zhao, and F. Su, "Scale aggregation network for accurate and efficient crowd counting," in Proceedings of the European Conference on Computer Vision (ECCV), pp. 734-750, 2018.
  - [12] J. Gall, A. Yao, N. Razavi, L. Van Gool and V. Lempitsky, "Hough Forests for Object Detection, Tracking, and Action Recognition," in IEEE Transactions on Pattern Analysis and Machine Intelligence, vol. 33, no. 11, pp. 2188-2202, Nov. 2011.
  - [13] K. Chen, C. C. Loy, S. Gong, and T. Xiang, "Feature mining for localised crowd counting," in British Machine Vision Conference (BMVC), vol. 1, no. 2, pp. 3, 2012.
  - [14] A. B. Chan, Zhang-Sheng John Liang and N. Vasconcelos, "Privacy preserving crowd monitoring: Counting people without people models or tracking," 2008 IEEE Conference on Computer Vision and Pattern Recognition, Anchorage, AK, 2008, pp. 1-7.
  - [15] V. Ranjan, H. Le, M. Hoai, "Iterative crowd counting," in Proceedings of the European Conference on Computer Vision (ECCV), pp. 270-285, 2018.
  - [16] Y. Li, X. Zhang and D. Chen, "CSRNet: Dilated Convolutional Neural Networks for Understanding the Highly Congested Scenes," 2018 IEEE/CVF Conference on Computer Vision and Pattern Recognition, Salt Lake City, UT, 2018, pp. 1091-1100.
  - [17] Z. Ma and A. B. Chan, "Crossing the Line: Crowd Counting by Integer Programming with Local Features," 2013 IEEE Conference on Computer Vision and Pattern Recognition, Portland, OR, 2013, pp. 2539-2546.
  - [18] C. Wang, H. Zhang, L. Yang, L. Si, and X. Cao, "Deep people counting in extremely dense crowds," in Proceedings of the 23rd ACM international conference on Multimedia, 2015, pp. 1299-1302.
  - [19] K. Simonyan and A. Zisserman, "Very deep convolutional networks for large-scale image recognition," arXiv:1409.1556 [cs.CV], Sep. 2014.
  - [20] D. Kong, D. Gray and Hai Tao, "A Viewpoint Invariant Approach for Crowd Counting," 18th International Conference on Pattern Recognition (ICPR'06), Hong Kong, 2006, pp. 1187-1190.
  - [21] M. Rodriguez, I. Laptev, J. Sivic and J. Audibert, "Density-aware person detection and tracking in crowds," 2011 International Conference on Computer Vision, Barcelona, 2011, pp. 2423-2430.
  - [22] M. Li, Z. Zhang, K. Huang and T. Tan, "Estimating the number of people in crowded scenes by MID based foreground segmentation and head-shoulder detection," 2008 19th International Conference on Pattern Recognition, Tampa, FL, 2008, pp. 1-4.
  - [23] J. Liu, C. Gao, D. Meng and A. G. Hauptmann, "DecideNet: Counting Varying Density Crowds Through Attention Guided Detection and Density Estimation," 2018 IEEE/CVF Conference on Computer Vision and Pattern Recognition, Salt Lake City, UT, 2018, pp. 5197-5206.
  - [24] V. A. Sindagi and V. M. Patel, "CNN-Based cascaded multi-task learning of high-level prior and density estimation for crowd counting," 2017 14th IEEE International Conference on Advanced Video and Signal Based Surveillance (AVSS), Lecce, 2017, pp. 1-6.
  - [25] K. He, X. Zhang, S. Ren and J. Sun, "Deep Residual Learning for Image Recognition," 2016 IEEE Conference on Computer Vision and Pattern Recognition (CVPR), Las Vegas, NV, 2016, pp. 770-778.
  - [26] G. Huang, Z. Liu, L. v. d. Maaten and K. Q. Weinberger, "Densely Connected Convolutional Networks," 2017 IEEE Conference on Computer Vision and Pattern Recognition (CVPR), Honolulu, HI, 2017, pp. 2261-2269.
  - [27] J. Dai, Y. Li, K. He, and J. Sun, "R-fcn: Object detection via region-based fully convolutional networks," in Advances in neural information processing systems, 2016, pp. 379-387.
  - [28] S. Ren, K. He, R. Girshick and J. Sun, "Faster R-CNN: Towards Real-Time Object Detection with Region Proposal Networks," in IEEE Transactions on Pattern Analysis and Machine Intelligence, vol. 39, no. 6, pp. 1137-1149, 1 June 2017.
  - [29] H. Idrees, M. Tayyab, K. Athrey, D. Zhang, S. Al-Maadeed, N. Rajpoot and M. Shah, "Composition loss for counting, density map estimation and localization in dense crowds," in Proceedings of the European Conference on Computer Vision (ECCV), pp. 532-546, 2018.
  - [30] V. Pham, T. Kozakaya, O. Yamaguchi and R. Okada, "COUNT Forest: CO-Voting Uncertain Number of Targets Using Random Forest for Crowd Density Estimation," 2015 IEEE International Conference on Computer Vision (ICCV), Santiago, 2015, pp. 3253-3261.
  - [31] B. Xu, N. Wang, T. Chen, and M. Li, "Empirical evaluation of rectified activations in convolutional network," arXiv:1505.00853 [cs.LG], 2015.
  - [32] B. Sheng, C. Shen, G. Lin, J. Li, W. Yang and C. Sun, "Crowd Counting via Weighted VLAD on a Dense Attribute Feature Map," in IEEE Transactions on Circuits and Systems for Video Technology, vol. 28, no. 8, pp. 1788-1797, Aug. 2018.

- [33] X. Glorot, and Y. Bengio, "Understanding the difficulty of training deep feedforward neural networks," in Proceedings of the thirteenth international conference on artificial intelligence and statistics, pp. 249-256, 2010.
- [34] T. Zhao, R. Nevatia and B. Wu, "Segmentation and Tracking of Multiple Humans in Crowded Environments," in IEEE Transactions on Pattern Analysis and Machine Intelligence, vol. 30, no. 7, pp. 1198-1211, July 2008.
- [35] L. Liu, H. Wang., G. Li, W. Ouyang, and L. Lin, "Crowd counting using deep recurrent spatial-aware network," arXiv:1807.00601 [cs.CV], 2018.
- [36] D. B. Sam and R. V. Babu, "Top-down feedback for crowd counting convolutional neural network," in Thirty-Second AAAI Conference on Artificial Intelligence, 2018.
- [37] Z. Shi et al., "Crowd Counting with Deep Negative Correlation Learning," 2018 IEEE/CVF Conference on Computer Vision and Pattern Recognition, Salt Lake City, UT, 2018, pp. 5382-5390.
- [38] A. G. Howard, M. Zhu, B. Chen, D. Kalenichenko, W. Wang, T. Weyand, M. Andreetto, and H. Adam, "Mobilenets: Efficient convolutional neural networks for mobile vision applications," arXiv:1704.04861 [cs.CV], 2017.